PERGAMON

International Journal of Solids and Structures 40 (2003) 3021–3037

INTERNATIONAL JOURNAL OF SOLIDS and STRUCTURES

www.elsevier.com/locate/ijsolstr

A failure criterion based on material instability

S.E. Schoenfeld *, T.W. Wright [1]

US Army Research Laboratory, AMSRL-WM-TD, Aberdeen Proving Ground, MD 21005-5066, USA

Received 16 July 2002

Abstract

Scaling laws for adiabatic shear bands are used to parameterize a model that is suitable for introducing shear damage within engineering calculations. One-dimensional solutions to the governing equations for a single shear band provide laws that connect the driving deformation, the imperfections, and the physical characteristics of the material to the process of stress collapse [International Journal of Plasticity 8 (1992) 583, Mechanics of Materials 17 (1994) 215]. The current model uses homogeneous material response and the scaling laws to anticipate the correct timing beyond the maximum stress at which stress collapse should occur. The model is implemented into a finite element code for wave propagation and used in the analysis of boundary value problems that are dominated by shear failure. Finally, implications of the model for simulations of material failure are discussed.

Keywords: Adiabatic shear bands; Failure modeling

1. Introduction

Observations of material failure during explosive and impact loading often include accounts of highly localized deformation that may either dominate or contribute to the failure event. Primarily concerned with the effects of secondary heat-treatment on ballistic limit velocity, Burkins et al. (1997, 2000) conducted a series of experiments involving a 20 mm fragment-simulating projectile fired at increasing velocity into nominally 1-in. thick plates of a titanium alloy (Ti–6Al–4V). In spite of the wide range in limit velocity attributed to the effects of secondary heat-treatments, an overwhelming number of specimens failed via "plugging" leading to break-out of large pieces of target material. Subsequent metallographic analysis of plates recovered from these experiments (Kad et al., 2000) document that break-out was preceded by large macroscale shear localizations leading to cracks, and eventually, the formation of plugs. Magness (1994) observed the relative propensity of some materials to localize during deep (semi-infinite) penetration experiments. Within this context, the extent of shear localization associated with material discard seemed to control the efficiency of the penetration process. Raftenberg and Krause (1999) report large numbers of

* Corresponding author. Tel.: +1-410-306-0800/0785; fax: +1-410-306-0783.
E-mail addresses: scotts@arl.army.mil (S.E. Schoenfeld), tww@arl.army.mil (T.W. Wright).
[1] Tel.: +1-410-306-1943; fax: +1-410-306-0661.

0020-7683/02/$ - see front matter © 2002 Elsevier Science Ltd. All rights reserved.
doi:10.1016/S0020-7683(03)00059-3

shear bands along the penetration cavity of steel plates perforated by shaped-charges while Erlich et al. (1980) report that fragments recovered after the explosion of steel casements are entirely surrounded by shear bands.

The preceding examples serve to underscore the technological importance of a broad class of failure via thermo-mechanical instability. This mechanism, which today is called adiabatic shear, has been known and studied for many years, and as such there is now a very large database from the perspectives of both materials science and mechanics. The literature now is too large to review thoroughly here, but some of the highlights may be mentioned. Zener and Hollomon (1944) were probably the first to recognize that rapid plastic working, accompanied by self-heating and subsequent strain softening, was an agent that could lead to material instability, which manifested itself as very narrow regions of intense shear. Prior to 1980, adiabatic shear was studied mostly from the viewpoint of materials science.

The works of Clifton (1980) and Bai (1982) inaugurated a new era of interest in the thermo-mechanics of the phenomenon. Merzer (1982) and Wright and Batra (1985), among others, approached the issue computationally as a one-dimensional problem and observed that with increasing strain, stress reached a maximum and then began a slow decrease followed by the initiation of a rapid collapse. Due to inadequate numerical resolution, only the beginning of the stress collapse could be observed in either of these works. Decreasing stress with increasing strain had long been thought to be inherently unstable, but in a visco-plastic material, the instability is not immediately apparent at peak stress, as these papers showed.

The torsional split-Hopkinson bar or Kolsky bar has become the principal experimental apparatus for examining the formation of adiabatic shear bands. Definitive experiments by Marchand and Duffy (1988) showed not only all the expected features of initial slow growth of stress, followed by peak stress, slow decay, and rapid collapse, but also included temperature measurements and images of the distribution of strain across the band. They also found that the shear band actually initiates at a point in the test section and then propagates around the tube.

Theoretical work was also developing along with the experimental and computational progress. Molinari and Clifton (1987) made an exact analysis of the torsional configuration for applied stresses on the boundary and an approximate analysis for applied velocities. Using a different approach, Wright (1990) made an exact analysis of the torsional problem for applied velocities. Both papers showed that the collapse strain decreases logarithmically with increasing size of the initial perturbation. The first paper simply plotted results for a perturbation in the thickness of the wall of the tube. The second paper gave a scaling law for the collapse strain and further showed that small initial perturbations in strength, temperature, and wall thickness may simply be added when each is properly scaled to give a total effective perturbation. Later Duffy and Chi (1992) confirmed experimentally that the critical strain at which stress collapse occurs is not a constitutive quantity but depends logarithmically on the size of initial geometric defects. By extension from the theoretical results, this confirms the nature of the functional dependence on other types of defect as well.

A broad survey was presented by Bai and Dodd (1992), and recently a monograph by Wright (2002) has covered theoretical aspects. Several symposia have appeared in the last decade as well. Work continues today on many aspects of adiabatic shear. Of particular interest are propagation (Kalthoff, 2000; Guduru et al., 2001), ensemble behavior (Grady and Kipp, 1987; Wright and Ockendon, 1996; Xue et al., 2001), and the final transition from shear band to crack for which little is known.

In spite of the enormous knowledge surrounding the problem of thermo-mechanical instability, very little of this information has transitioned into failure models for engineering design. We find this quite surprising when one considers on one hand the technological "pull" of the design engineer faced with an environment dominated by thermo-mechanical instability and on the other hand the intellectual "push" from many years of academic activity.

Among the most basic failure "criteria" we find that engineering practice often specifies critical values of strain or stress and considers that failure has taken place once the local material state exceeds one or the

other of such criteria. For ductile materials, the criterion of critical "effective" or "deviatoric" strain may seem compelling, but in fact, is not well suited to general analysis of materials deforming rapidly.

Among general engineering considerations of material failure, we find models such as that proposed by Johnson and Cook (1985) have enjoyed very broad implementation within the community of high strain-rate analysis (e.g., EPIC, CTH, LS-DYNA, DYNA2D/3D, etc). This model seeks to "evolve" damage within a material as a function of strain, strain rate, temperature, and triaxiality (ratio of mean to deviatoric stresses). The model offers no physical basis for the eventual failure but seeks (through a large experimental database) to give a phenomenological description of the strain and loading conditions under which failure is known to occur. Failure due to adiabatic shear is accounted for by including experiments dominated by thermal instability within the database, typically experiments involving torsion of thin-walled specimens deformed at high rates (torsional split-Hopkinson bar experiments).

Other attempts have been made to include concepts of material stability into the failure modeling of materials. The criterion for a stable work-hardening material (Drucker, 1959) corresponds to roughly the strain at maximum true stress. Becker (2002) implemented the Drucker stability limit as a strain-to-failure criterion. Following Saje et al. (1982), Becker also developed a separate criterion based on the bifurcation analysis of Rice (1976). He then compared the two criteria in simulations of an expanding ring finding the Drucker concept better suited to his particular analysis. It should be noted here that even though the underlying physics of material damage was due to void growth, ultimate failure was determined based on a macroscopic stability criterion.

Raftenberg (2001) developed a failure strain due to adiabatic shear as the amount of additional strain beyond the point of peak stress when instabilities would grow and dominate material behavior. This was left as a parameter to be determined via experimental Hopkinson bar techniques. In light of the current understanding that such techniques are sensitive to small defects, it seems unlikely, or at least improbable that such a parameter will be developed without reference to inherent defects in the experimental technique.

More recent work yet has been focused on structural mechanisms rather than on local materials instability, although the two are certainly related. For example, see Li and Jones (2002) and other works referenced therein.

The work by Curran et al. (1987) summarizes the authors' earlier efforts at introducing a physical basis for failure by adiabatic shear. Described as a theory for "microstatistical fracture mechanics," the work describes damage due to adiabatic shear localization as one of many microstructure-based damage mechanisms competing to degrade the mechanical properties of solids. As deformation proceeds toward achieving peak stress, shear bands are considered to nucleate and grow in large ensembles. These bands then grow and coalesce (Curran and Seaman, 1986) to form macroscopic failure. While the model does consider multidimensional damage leading to anisotropy, the nucleation law seems to require a density of initial defects that is unrealistically large. In this model, emphasis is placed on the statistics of microstructural features and response of these features to externally applied loads. The resulting model is complicated, requiring considerable experimental effort to calibrate and is of questionable utility outside the calibrated bounds. Further, exhaustive and detailed comparison with recovered microstructures has shown that the defect growth must be artificially limited, and reasonable bounding laws have yet to be determined.

The proposed model will stand in stark contrast to methods that attempt detailed accounting of defect structures within the material. Our description for damage due to shear bands is an attempt to generalize a simple, but in this case physically representative problem of stress collapse during the simple shearing of a narrow strip of rigid/plastic material. This description is intimately tied to the material and geometric defects that initiate stress collapse, but our emphasis will be on problems governed by geometrically driven variations in the velocity field as may occur during machining or penetration of metals. That is not to say that our model is unaware of defects within the material; such defects would be strongly emphasized within the homogeneous behavior as defined by the material's constitutive response. Our model however, will

provide the macroscopic linkage between the "softening" or "damaging" material and the ultimate loss of stress carrying capability that arises in the context of the technologically important class of problems that involve strong discontinuities and/or much weaker velocity gradients.

The current review of our model proceeds with a summary for the criterion of stress collapse due to adiabatic shear. The problem of simple shearing is reviewed and the details of ultimate stress collapse are described as a function of both the driving imperfections and the homogeneous response of a work-hardening, strain-rate hardening and thermally softening material. We will describe a simple generalization of this scheme to formulate a macroscopic failure model for damage due to shear localization and the incorporation of this more general model within the context of finite element analysis techniques. We will exercise the model by way of example problems designed to highlight strengths and weaknesses in the current formulation and to understand its appropriateness for describing failure for a certain class of materials and driving conditions. Finally we will summarize our model and describe some of its current assumptions as well as general directions for further development.

2. Summary of a criterion for adiabatic shear

The ideas, upon which the numerical model for initiation of an adiabatic shear band in this paper is based, were developed in two papers some eight to ten years ago, (Wright, 1992, 1994) and have also been discussed in a recent comprehensive summary (see Wright, 2002). However, we only recently recognized that the earlier papers actually contained the beginnings of an idea that could be developed into a computational failure model. These ideas will be outlined in this section; for further details, the reader may refer to the original papers.

Consider the dynamic response of a thin-walled tube in torsion, as experienced by a specimen in a Kolsky bar experiment. Fig. 1 illustrates the typical response of a work-hardening material. In slow loading, or if adiabatic heating is somehow suppressed, the material may show continuous hardening out to large shear strains, as indicated by the upper curve in the figure. However, plastic working will heat the material, and because metals tend to soften with increasing temperature, eventually the flow stress will reach a maximum at $\gamma_{\max\ \text{stress}}$, followed by strain softening, as indicated schematically by the middle curve. In a perfect material with perfectly uniform distributions of stress, strain, and temperature, softening may continue indefinitely.

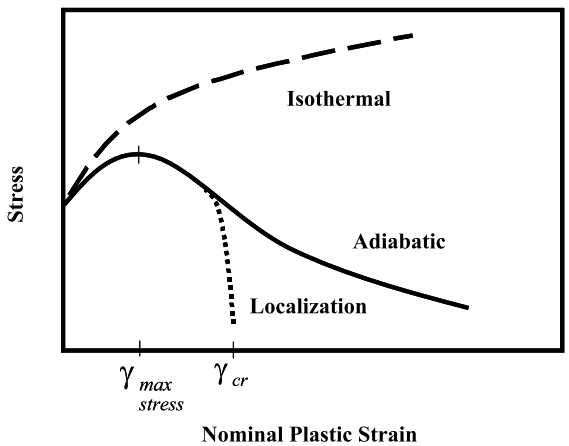

Fig. 1. Shear stress versus nominal shear strain for a typical work-hardening material during a torsion experiment.

No real material in a real experiment has perfectly uniform distributions of the fields, however. Instead there will be fluctuations and concentrations in the specimen due to boundary conditions, specimen design, wave propagation, or internal imperfections in the material structure. Indeed, nonuniform distributions may arise from many different sources, and because strain softening is inherently unstable if the rates are high enough, localization may occur eventually at the most prominent nonuniformity. At some nominal critical strain, γ_{cr}, the straining and heating at the most critical point will tend to run away while the straining and heating at all other nearby points comes to a stop. The mathematical problem has two parts. First, for given initial conditions in the one-dimensional problem, determine the difference between the critical strain and the strain at maximum stress. Second, generalize the result to three-dimensional problems in a properly invariant way.

After nondimensionalization in the most straightforward way (see Wright, 1992 for details) the one-dimensional problem may be written as follows

$$\begin{aligned} s_y &= \rho v_t, \\ \theta_t &= k\theta_{yy} + s v_y, \\ \kappa_t &= M(\kappa,\theta) s v_y, \\ s &= F(\kappa,\theta,v_y). \end{aligned} \tag{1}$$

The nondimensional field variables are the shear stress s, the velocity v, the temperature θ, and a work-hardening parameter κ. The last parameter corresponds to the current yield stress at the initial ambient temperature. Nondimensional density and thermal conductivity are constants ρ and k, respectively. Constitutive functions M and F determine the rate of work hardening and the flow stress, while subscripts indicate partial derivatives with respect to the variable indicated.

The homogeneous adiabatic solution to Eq. (1) may be written

$$s = S(t), \quad \theta = \Theta(t), \quad \kappa = K(t), \quad v = y \tag{2}$$

and follows from the solution of the coupled ordinary differential equations to which (1) reduces when the general form (2) is inserted into the equations. Once the homogeneous solution is known, perturbation equations may be found by assuming that a solution that is a close neighbor to the homogeneous one may be written as $s = S(t) + \tilde{s}(y,t)$, etc., where the tilde indicates a small quantity in some appropriate sense. By use of standard methodology, perturbation equations are found by inserting these new forms for the field quantities into (1) and keeping only the lowest order terms. The result for the quasistatic case is

$$\begin{aligned} \tilde{s}_y &= 0, \\ \tilde{\theta}_t &= k\tilde{\theta}_{yy} + \tilde{s} + S\tilde{v}_y, \\ \tilde{\lambda}_t &= M_\kappa S\tilde{\lambda} - kM\tilde{\theta}_{yy}, \\ \tilde{s} &= F_\kappa\tilde{\lambda} + \frac{\mathrm{d}S}{\mathrm{d}\theta}\tilde{\theta} + mS\tilde{v}_y, \end{aligned} \tag{3}$$

where $\tilde{\lambda} = \tilde{\kappa} - M\tilde{\theta}$ and the strain-rate sensitivity is given by $m = F_{\dot{\gamma}}/F$. The important point to notice here is that terms in capital letters, such as S, M, F, and their derivatives all depend on the homogeneous solution and so are known functions of time. If the thermal conductivity is finite, the equations are difficult to handle, because of the coupling. If $k = 0$, however, there is considerable simplification and explicit solutions may be written down that give considerable insight to their general behavior. With the further specializations that m is constant and M depends only on κ, the result is

$$\begin{aligned}
\tilde{s} &= 0,\\
\tilde{\lambda} &= \frac{M}{M_0}\tilde{\lambda}_0,\\
\tilde{\theta} &= \tilde{\theta}_0 S^{-1/m} - \frac{\tilde{\lambda}_0}{mM_0}\int_0^t F_\kappa M\left(\frac{S(t')}{S(t)}\right)^{1/m} \mathrm{d}t',\\
\tilde{v}_y &= -\frac{1}{mS}\left(F_\kappa\tilde{\lambda} + \frac{\mathrm{d}S}{\mathrm{d}\theta}\tilde{\theta}\right).
\end{aligned} \tag{4}$$

Results concerning finite thermal conductivity and more general forms for m and M may be found in Wright (1992). The fundamental character of the solution is not altered by these generalizations, however.

Eq. (4) shows several important effects that are characteristic of solutions to (3). First note that the perturbation in stress vanishes exactly. This means that the perturbed stress follows the same path as the unperturbed stress, at least initially, but that initiation of the collapse of stress, which eventually occurs in the fully developed band, cannot be captured by the perturbation equations. Next note that because the strain-rate sensitivity is small, the solution for the perturbation in temperature shows that there must be an initial boundary layer in time when S is an increasing function as in work-hardening materials. The boundary layer should be regarded as a mathematical artifact only since no realistic loading will arrive with the abrupt initial conditions that must be assumed for the perturbed problem. In fact, it is possible to choose initial conditions in such a way that the boundary layer is suppressed, but doing so results in no significant difference in the time of localization.

Asymptotic analysis of the integral in (4) allows algebraic estimates to be written for each of the perturbed fields as the solution leaves the boundary layer (see Wright, 1992 for details). The most important result is $\tilde{\theta} \sim -\tilde{\lambda}F_\kappa/S_\theta$ with $\tilde{\lambda}$ given in (4). Thus, once the homogeneous solution is known, the most important features of any perturbed solution are also known. These all have the form $\tilde{\lambda}_0$ times a known function of time. Since $\tilde{\lambda}_0(y) = \tilde{\kappa}_0(y) - M_0\tilde{\theta}_0(y)$, the effective solution depends only on a linear combination of initial conditions rather than on each one independently. Such behavior is typical in problems with boundary layers.

In a work-hardening material, the adiabatic stress S, reaches a maximum at some temperature and plastic strain, and therefore, because the denominator of the expression for $\tilde{\theta}$ vanishes there, the asymptotic result breaks down and must be replaced by a more refined estimate near the peak stress. The final results are more complicated than indicated above, but they are still only algebraic expressions with the form $\tilde{\lambda}_0$ times a known function of time. Details are given in the references.

Even though the perturbed stress cannot determine the moment of stress collapse, an estimate may still be obtained by finding the time when the perturbed strain rate is equal to the nominal imposed rate so that the linearized results will surely have failed. That is, find the time when $\tilde{v}_y = 1$, or in dimensional terms when $\partial v/\partial y - \dot{\gamma}_0 = \dot{\gamma}_0$ so that the perturbation is no longer small. The result from the linearized equations is

$$\eta e^{\eta^2}(1 + \operatorname{erf}\eta) = \frac{1-\beta}{\sqrt{\pi}\beta}, \tag{5}$$

where η is a scaled measure of the distance past peak stress, and β is a scaled measure of the strength of the perturbation,

$$\begin{aligned}
\eta &= \sqrt{(-S_{\theta\theta}/2mS)_{\max}}(\Theta_{\mathrm{cr}} - \Theta_{\max}) = \sqrt{(-S_{\gamma^p\gamma^p}/2mS)_{\max}}(\gamma^p_{\mathrm{cr}} - \gamma^p_{\max}),\\
\beta &= -\left(\frac{F_\kappa M}{mSM_0}\right)_{\max}\tilde{\lambda}_0 = \tilde{v}_y(0, t_{\max}).
\end{aligned} \tag{6}$$

In Eq. (6), the subscript *max* indicates that the quantity is to be evaluated at the point of maximum adiabatic stress. In the second expression for η, effective plastic strain has replaced the homogeneous temperature as the independent variable by virtue of the nondimensional adiabatic relation $d\Theta = S d\gamma^p$. One result from the asymptotic solution is that the defect, β, may be directly related to the perturbation of velocity at peak stress, as well as to initial conditions. This fact will prove useful in developing the failure model for general loadings. The derivation of Eq. (5) is such that it is expected to be most accurate as a solution to $\tilde{v}_y = 1$ at the point $\eta = 0$, $\beta = 1$. Eq. (5) is plotted as the lower curve in Fig. 2.

In fact, because (5) was derived from linearized equations, it is extremely unlikely to deliver valid results for the actual nonlinear problem. However, it does suggests that there may be a simple relation between the critical strain, when properly scaled, and a scaled defect

$$\eta = f(\beta). \tag{7}$$

Furthermore, it suggests that only a single scalar measure of the defect need be considered and that the defect may be regarded either as a scaled, composite, initial condition or as the perturbation in velocity gradient at peak stress.

In order to test the suggested hypotheses in the previous paragraph numerical calculations were made for a wide variety of physical parameters and initial conditions in the fully nonlinear problem including heat conduction (see Wright, 1994). It was verified that the composite defect, rather than considering strength and temperature defects individually, gives an accurate result up to $|\tilde{\lambda}_0| \approx 0.035$. These results are also plotted in Fig. 2. Except for two points for which the peak stress lay within the initial boundary layer and thus should be discarded, all points lie near the tangent to Eq. (5) that passes through the origin of the figure. This tangent line may be expressed as

$$\eta = \frac{1}{\sqrt{\pi}} \ln \frac{1}{\beta}, \tag{8}$$

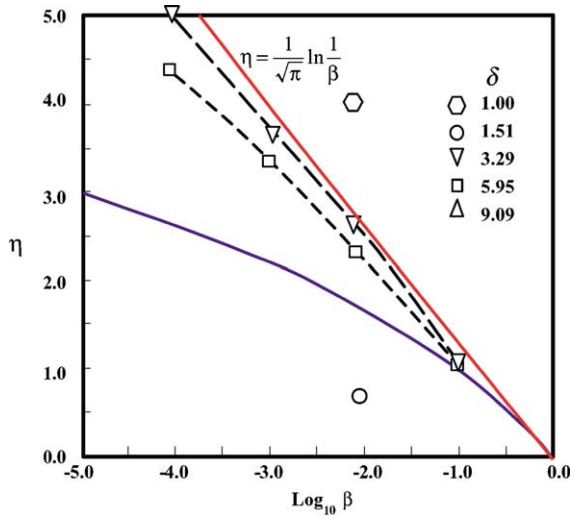

Fig. 2. Scaled distance beyond peak stress as a function of perturbation strength and initiating defect. Blue line represents the estimate from the linearized solution for the quasistatic and nonheat conducting case while the dashed lines represent numerical solutions to the fully coupled situation. Red line presents a representative organization over a broad range of material parameters presented by $\delta = n/m(1+n)$. Figure is reproduced from Wright (1994).

or in dimensional form as

$$\gamma^p_{\rm cr} - \gamma^p_{\rm max} = \sqrt{\left(\frac{2mS}{-\pi S_{\gamma^p\gamma^p}}\right)_{\rm max}} \ln \frac{m}{\left(\frac{-s_\theta}{S}\right)_{\rm max}\left(\theta_0 - \frac{\gamma_0}{n\rho c}\kappa_0\right)}$$
$$= \sqrt{\left(\frac{2mS}{-\pi S_{\gamma^p\gamma^p}}\right)_{\rm max}} \ln \frac{\dot\gamma_0}{(v_y)_{\rm max} - \dot\gamma_0}. \tag{9}$$

The first line of Eq. (9) corresponds to use of the initial defects, whereas the second line corresponds to the variation of the velocity gradient at peak stress. The two forms are entirely equivalent, as indicated by the second line in Eq. (6). The subscript *max* in the equations means that the quantity is to be evaluated at the peak of the adiabatic stress–strain curve where $\mathrm{d}S/\mathrm{d}\gamma^p = 0$. The terms γ_0 and n are used to fit the basic work-hardening response, $\kappa(1+\gamma/\gamma_0)^n$, and θ_0 and κ_0 are the initial defects in temperature and strength at a point.

Note that the curvature of the adiabatic response has a large effect on the critical strain, as does the strain-rate sensitivity. Also note that the term s_θ in the denominator of the first logarithmic term refers to the rate of softening at a fixed value of the hardening parameter, not the total rate of change of the adiabatic response with temperature. Recall that the nondimensional flow stress at a fixed strain rate is given as $s = F(\kappa,\theta,1)$ and that the adiabatic response is given by $S(\Theta) = F(K(\Theta),\Theta,1)$. Therefore, at the point where $S_\Theta = 0$, according to the last two of Eq. (1), we have $F_\theta + F_\kappa M = 0$ or $s_\theta \equiv F_\theta = -F_\kappa M$.

3. Numerical implementation

So far a description of the initiation time or strain in a one-dimensional problem has been described. The generalization to three-dimensions adopted in this paper is perhaps the simplest possible. Because the perturbed stress is virtually identical to the adiabatic stress, it is only necessary to find the peak in the adiabatic response, which for a given strain rate and flow law occurs at a fixed equivalent plastic strain. Because the one-dimensional problem has been stated as a shearing problem, the appropriate definition for equivalent plastic strain is $\gamma^p = \gamma^p_0 + \int_0^t \dot\gamma^p \,\mathrm{d}t'$ where $\dot\gamma^p = (2\mathbf{D}^p:\mathbf{D}^p)^{1/2}$ and $\mathbf{D}^p$ is the plastic part of the stretching tensor. Thus, $\dot\gamma^p$ is the equivalent plastic strain rate in shear. Likewise, we take $S = (\frac{1}{2}\mathbf{S}:\mathbf{S})^{1/2}$, where $\mathbf{S}$ represents the deviatoric portion of the Cauchy stress tensor, to be the equivalent measure of stress normalized with respect to a shearing test. Typical data for material behavior is often reported in quantities normalized with respect to tension. Likewise, many numerical implementations require such data in the form of $\sigma^e = (\frac{3}{2}\mathbf{S}:\mathbf{S})^{1/2}$ and $\dot\varepsilon^p = (\frac{2}{3}\mathbf{D}^p:\mathbf{D}^p)^{1/2}$, so-called "effective" stress and "effective" strain. In terms of effective measures, (9) is simply

$$\varepsilon^p_{\rm cr} - \varepsilon^p_{\rm max} = \sqrt{\left(\frac{2m\sigma^e}{-\pi\sigma^e_{\dot\varepsilon^p\dot\varepsilon^p}}\right)_{\rm max}} \ln\frac{1}{\beta}. \tag{10}$$

Generalization of the nondimensional velocity perturbation, β, seems to be most straight forward when interpreted as variation in effective strain rate within the neighborhood of any particular element (with respect to a typical finite-element discretization). As soon as the maximum stress has been reached in the ith element, the perturbation is calculated from

$$\beta^i = \frac{\dot\varepsilon^i - \dot\varepsilon^{\rm avg}}{\dot\varepsilon^{\rm avg}} \geqslant 0 \quad \text{where } \dot\varepsilon^{\rm avg} = \frac{1}{\alpha}\sum_{j=1}^{\alpha}\dot\varepsilon^j \tag{11}$$

and α is determined by the connectivity of elements so as to include all neighboring elements. Here we have considered not just local strain rate, but the simple average of strain rates in the surrounding region as the

background against which we measure fluctuations. Thus, our focus here will be on perturbations in the velocity field that arise in the context of the macroscopic boundary value problem and not within the context of internal imperfections in the material structure.

Assuming that loading is monotonic, Eq. (10) is evaluated at conditions of peak adiabatic stress. In the context of explicit integration schemes and multi-axial stress conditions, resolution of the exact time of peak conditions can be a difficult task. For instance, the criterion for a stable inelastic material proposed by Drucker (1959),

$$\dot{\sigma}_{ij}\dot{\varepsilon}_{ij} \geqslant 0 \tag{12}$$

corresponds roughly to the maximum true stress. It would be appealing to monitor constitutive response within each element for the condition of (12), but the criterion is susceptible to unloading during path changes or wave reflections. The method implemented by Raftenberg (2001) employs the constitutive equation, $\sigma^e = f(\varepsilon^p, \dot{\varepsilon}^p, \theta)$, and the nonheat conducting version of the second of Eq. (1) in an iterative scheme to solve for the plastic strain at peak stress. Within the context of explicit wave-propagation analysis, this would be required for every gauss-point at each time-step and become a significant computational burden. Our approach has been to integrate the constitutive model over a range of strain rates prior to each calculation. During this process, the quantities $\varepsilon^p(\dot{\varepsilon})_{\max}$, $\sigma^e(\dot{\varepsilon})_{\max}$, and $\sigma^e_{\varepsilon^p\varepsilon^p}(\dot{\varepsilon})_{\max}$ are calculated and stored in the form of a lookup table. During calculations, necessary values at the current rate are extracted from this table using numerical interpolation and used to determine the state of the material with respect to conditions at peak stress (for a fixed rate) parameterized by ε^p. The preceding methodology has been implemented into the elastic plastic impact calculations (EPIC; Johnson et al., 1997) finite-element software. The program uses an explicit technique for forward integration of the equations of motion that is specifically well suited for impact and wave-propagation analysis.

4. Example calculations

In this section the generalized model is explored by way of example calculations specifically designed to highlight strengths and weaknesses in our approach. Our calculations will incorporate a modified Johnson and Cook (1983) description for the homogeneous behavior of a Ti–6Al–4V (Weerasooriya et al., 2001) alloy. The functional form of this equation is given by

$$\sigma^e = [C_1 + C_2(\varepsilon^p)^n][1 + C_3 \ln(\dot{\varepsilon}^p/\dot{\varepsilon}_0)]\left[1 - \left(\frac{\theta - \theta_{\text{room}}}{\theta_{\text{melt}} - \theta_{\text{room}}}\right)^M\right], \tag{13}$$

where $\dot{\varepsilon}_0$ represents a reference rate of shearing (taken here as 1.0) and θ_{melt} and θ_{room} represent melt and reference temperature respectively. The constitutive parameters were fit to data from compression tests using Instron and split-Hopkinson bar apparatus with the following results C_1 and C_2 are 1.035 and 0.889 GPa respectively while n and C_3 were found to be 0.4 and 0.015 respectively. M was taken to be 0.8 so as to be consistent with known yield strength versus temperature data for a number of other Ti–6Al–4V alloys.

4.1. Uniaxial compression

A computational grid of 3200, single gauss-point, triangular finite elements were used to represent a 1 cm × 1 cm compression sample. The specimen was deformed in two-dimensional plane-strain between two high-strength steel platens each moving with a fixed velocity of 10 m/s. Recall that our model depends intimately on variations in velocity that arise due to nonuniform deformations. When the model is run using simple sliding-only contact conditions, perturbations in velocity throughout the specimen are actually

quite minimal and, as a result, our specimen deforms uniformly without localized failure. The details of this result are omitted here for the purposes of space and brevity. The more interesting case arises when a small amount of friction is added to the contact conditions between the platens and the specimen. Here the nodal force that resists sliding is assumed equal to 0.02 (coefficient of friction, μ) of the force acting in the compression direction. Fig. 3 shows such a calculation. Due to planar symmetry, only one half of the calculation is displayed in this and subsequent figures. As shown in Fig. 3, after a compressive strain of 0.232, nonuniform deformations are firmly established as a result of frictional contact between the specimen and platens. Note here that the region of highest plastic strain and strain rate are the exterior corners at the specimen–platen interface. Calculated effective stresses for the sample are shown in Fig. 4 for various compression strains. At $\varepsilon = 0.232$, the effective stresses remain almost uniform (within the resolution of displayed contour values), while after $\varepsilon = 0.240$ compression, failure (sudden drop in effective stress) can be seen to initiate in the region of highest plastic strain and highest local variation in strain rate. After this time, the failure propagates through the interior of the specimen following directions of maximum effective strain and strain rate.

By varying the frictional conditions ($\mu = 0.00$, 0.02, 0.05 and 0.10) between the specimen and the platens, we also create conditions of increasing velocity gradient along this interface. These conditions are shown in Fig. 5. The figure shows true compressive stress (total compressive force normalized by the current area under the platen) versus true compressive strain for the bulk sample deformed under the different conditions. Increasing frictional force yields a slight increase in stress (as specimen expansion along the interface is inhibited) and increases stress and strain concentrations. Fig. 5 also contains contours of $\bar{\varepsilon}^p$ for each case just prior to the onset of material failure. Note that both the macroscopic strains to failure and the local

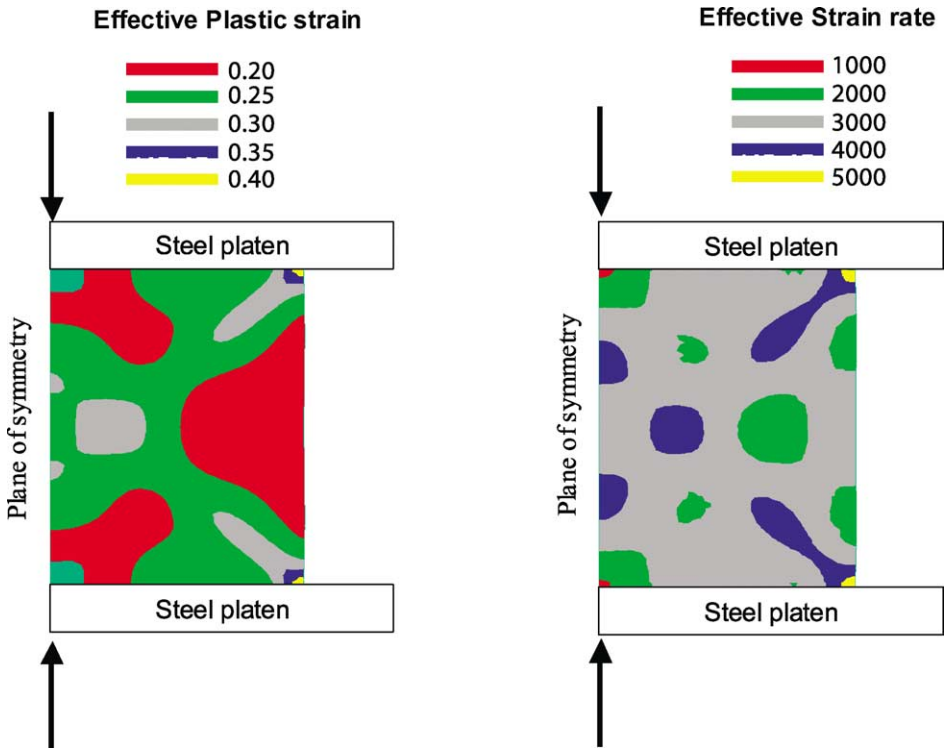

Fig. 3. Contours of effective plastic strain and strain rate after a compressive strain of 0.232 with $\mu = 0.02$.

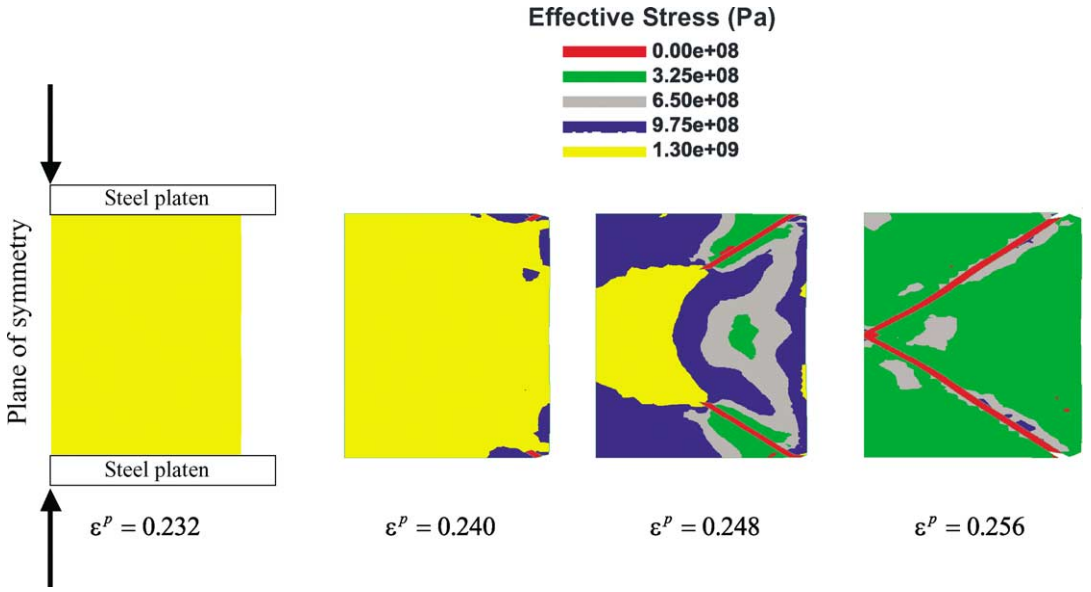

Fig. 4. Contours of effective stress for a Ti–6Al–4V cylinder with frictional contact conditions of $\mu = 0.02$. Contours are shown at nominal strains of 0.232, 0.240, 0.248, and 0.256.

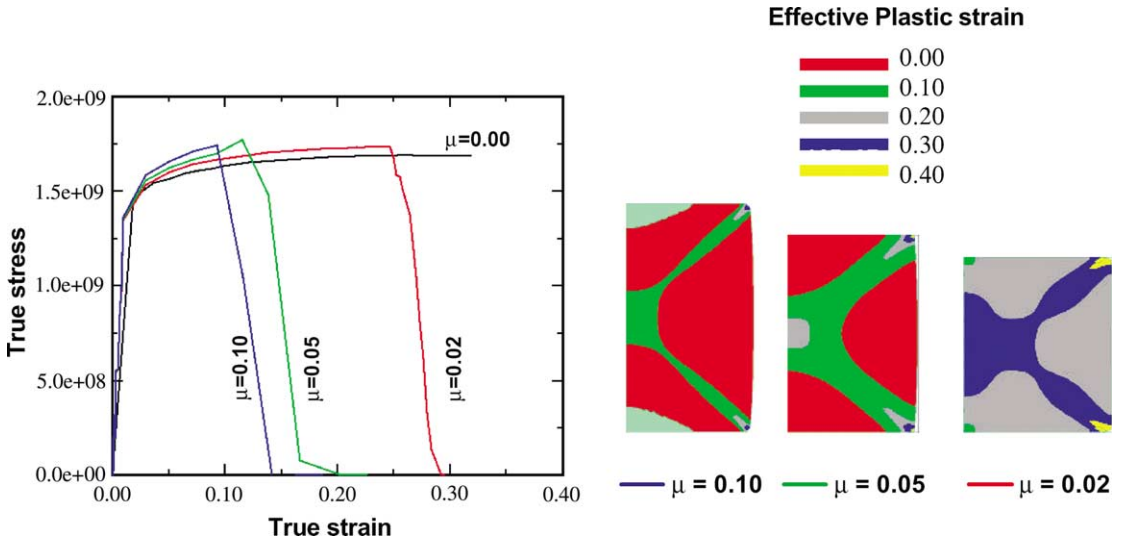

Fig. 5. Contours of effective plastic strain corresponding to the onset of material failure for three different contact conditions, $\mu = 0.10$, 0.05, and 0.02. Initiation of the failure process corresponds to macroscopic compressive strains of 0.05, 0.10, and 0.24.

strains just prior to failure decline significantly in context of increasing μ, or in other words, increasing variations in local strain rate.

4.2. Simulated edge impact

The sharp discontinuity in velocity caused by a projectile edge or the edge of a cutting tool creates a severe environment often associated with adiabatic shear localization. As determined by geometry, the location of an adiabatic shear failure is trivially understood and presents the possibility of explicitly resolving the competing effects of strain-rate hardening, work hardening, and heat conduction against thermal softening. In this example, we examine the sudden application of such a discontinuity and compare our model to results that arise from a highly resolved calculation. Fig. 6 compares results from two contrasting numerical descriptions of this problem. A 2.5 mm × 8 mm computational domain is subjected to a sharp velocity discontinuity along the left edge of the domain. Nodes located along the top half of the edge are instantaneously subjected to a constant velocity of 10 m/s while nodes along the lower half of the edge are subjected to a velocity of −10 m/s. Along the top, bottom, and opposite sides of the domain are transmitting boundary conditions that allow stress waves to pass through without reflection thus simulating a semi-infinite domain.

The calculation is conducted first considering both heat conduction and explicit wave propagation. A computational grid of 15,000 4-node quadrilateral elements were arranged so as to provide high resolution in the region of highest shearing. These elements are as small as 2 μm in the center region. Fig. 6(a) shows contours of shear stress emanating from the imposed velocity discontinuity and propagating across the mesh from left to right. Because of the high resolution of this mesh, and the scale of Fig. 6(a), stress contours along the centerline are not easily visible. Fig. 7 plots effective stresses along the centerline of the mesh.

By contrast, a purely mechanical calculation that neglects heat conduction is also presented. Here we assume nearly adiabatic conditions and convert 90% of the plastic work into local heating, but do not account for heat conduction away from the deforming material. The computational domain is shown in Fig. 6(b). In this case we consider 640 single gauss-point elements arranged in a crossed-triangle configuration and incorporate our model for failure via adiabatic shear damage. It should be noted here that this is

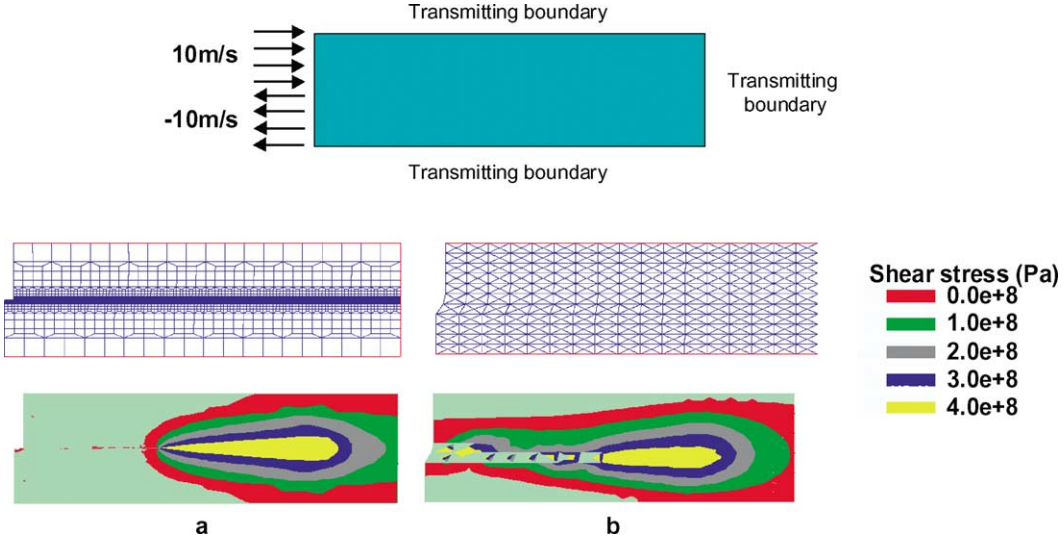

Fig. 6. A 2.5 mm × 8 mm computational domain with stress transmitting boundary conditions along three edges. The left edge is subjected to 20 m/s discontinuity in velocity. The figure contrasts (a) 15,000 elements with heat conduction to (b) a 640 element purely mechanical analysis. Contour plots show shear stress 10 μs after application of the velocity discontinuity.

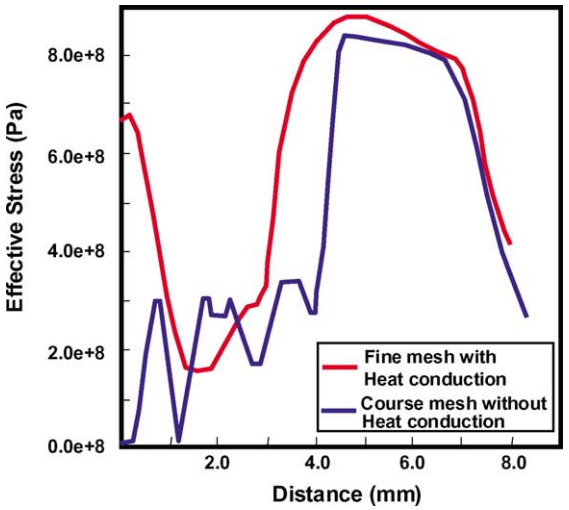

Fig. 7. Effective stress versus distance along the (horizontal) centerline for the two different numerical models of the edge impact problem in Fig. 6.

the desired element configuration and numerical framework used in many impact and penetration calculations and recommended by the EPIC authors. In this case, we use a uniform mesh to depict wave propagation away from the initial discontinuity. Note that on the coarse-scale (stress contours of Fig. 6(b)), stress contours near the leading edge of propagation appear almost identical to those of the more highly refined mesh. Behind the stress peak, we can see that triangles with gauss-points close to but not well aligned along the horizontal centerline do not always fail, leading to a certain amount of "noise" behind the initial stress pulse. Contrasts in such details become more evident when we directly examine stresses along the horizontal centerline in both meshes.

As previously mentioned, Fig. 7 shows effective stress along the horizontal centerline (distance as referenced from the applied velocity jump) of the computational domain depicted in Fig. 6. Far away from the applied velocity ($x > 8.5$ mm), wave propagation has not yet caused stresses to rise. Moving closer to the applied velocity ($7 < x < 8$ mm), stresses in both calculations rise steeply, however, the fine-scale calculation can be seen to rise more rapidly. This should be expected due to the overall higher mesh resolution. Both calculations depict the initial yield near 800 MPa. After yield ($4.5 < x < 6.75$ mm), localizing features in the fine-scale calculation begin to develop. We see that stresses grow as strain rate begins to climb, strain begins to accumulate and work hardening also contributes to increased stress. After reaching a peak stress ($x \approx 4.8$ mm), the fine-scale calculation shows that thermal softening slowly dominates, thus gently reducing stresses behind the initial pulse. Further behind the pulse ($x \leqslant 4$ mm), heat conduction begins to mitigate the effects of softening due to large temperature increases. Finally, the stress again begins to rise as we approach the boundary where velocities are applied. This is due to the presence of a purely mechanical condition at the boundary.

After an initial yield, work hardening is clearly seen within the coarse-scale calculation. Because we are not resolving the actual shear band, strain rates in the region between $4.5 < x < 6.75$ mm remain modest and stress levels could never be expected to reach those depicted in the fine-scale calculation. Note that for the current model, the amount of strain beyond the strain at peak stress varies inversely to velocity variations in the material neighborhood. Thus, for a very strong discontinuity, one would expect that the additional strain carried beyond the peak stress is very small. This situation is evident for the coarse-scale mesh as we see very little material softening prior to stress collapse in Fig. 7. The stress collapse is abrupt,

and any remaining stress carrying capability after the peak is simply due to misalignment of gauss-points with the actual shear band that occurs in the coarse mesh. We capture the width of the stress pulse from the leading edge to the peak stress, but not the details of stress decay beyond the peak. When one considers the volume of material actually involved in softening for the fine mesh, errors in the pulse width during softening may not significantly contribute to the global energy balance.

4.3. Plugging due to fragment impact

The preceding example was intended to contrast the proposed methodology with that of a more rigorous numerical analysis. From a technological perspective, the rigorous analysis is not always feasible due to the required generality of techniques and huge computational resources that would be required to conduct very broad analyses. Thus we find the need for a macroscale model that can depict damage due to shear bands.

For the final example, we consider the more technologically relevant analysis of a steel fragment impacting a plate of Ti–6Al–4V. The fragment, incident at 800 m/s normal to the plate, consists of a 20 mm diameter × 20 mm long right-circular cylinder while the plate is 25.4 mm in thickness. Such conditions are ideal for plugging via adiabatic shearing. The fragment is composed of 800 single gauss-point elements arranged in a crossed-triangle configuration. Likewise the plate is composed of 6400 such elements. In this example, we wish to compare the results of our model with those of prior established methodologies, in this case the framework originally proposed by Johnson and Cook (1985). Within this framework, damage is said to accumulate with respect to an instantaneous fracture strain, ε^f, where

$$\varepsilon^f = [D_1 + D_2 \exp(D_3\sigma^*)][1 + D_4 \ln(\dot{\varepsilon}^p/\dot{\varepsilon}_0)]\left[1 + D_5\left(\frac{\theta - \theta_{\text{room}}}{\theta_{\text{melt}} - \theta_{\text{room}}}\right)\right]. \tag{14}$$

σ^* is the ratio of mean to effective stress (triaxiality). Damage is represented as a single parameter that accumulates during each integration cycle as $D = \sum \Delta\varepsilon/\varepsilon^f$, where $\Delta\varepsilon$ is the total effective strain during each time increment. Once $D = 1.0$, the material is no longer allowed to carry hydrostatic tension or deviatoric stresses. It should be noted here that while this model has recently been extended by Børvik et al. (2002) for application to steel targets, its nature as dependant on a fixed strain-to-failure "state-variable", and thus

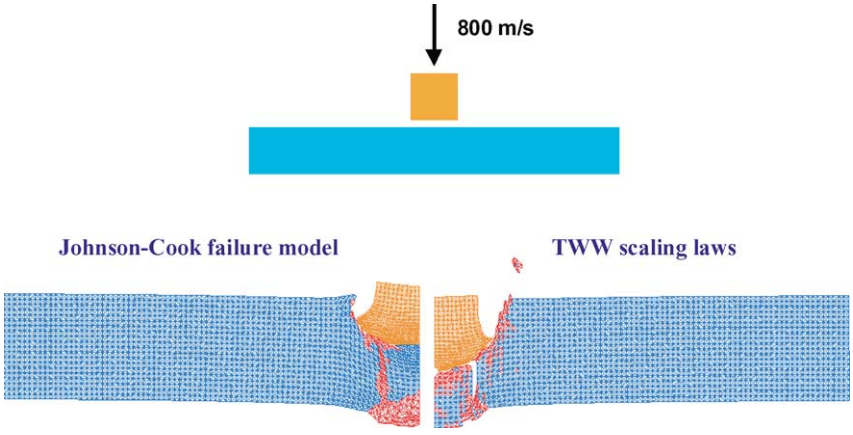

Fig. 8. Deformed geometry 70 μs after impact of a steel fragment on a Ti–6Al–4V plate. The left side shows calculated results using the Johnson and Cook (1985) fracture model while the right side shows deformed geometries using the current failure model. Elements colored in red have already failed while elements with an effective strain greater than 2.0 have not been drawn (and have also failed).

highly data dependent, has not been significantly altered. As such, for purposes of comparison to our model, we will maintain the form originally proposed by Johnson and Cook (1985).

As described in Johnson and Cook (1985), the five material parameters are fit to torsion, compression, and notched-bar tension data over a range of strain rates. Thus, the model is phenomenological and data intense. In Fig. 8, we compare two deformed geometries resulting from calculations that incorporate either the Johnson–Cook fracture model or the current model. Elements colored red are elements that have failed as a result of damage. Fully damaged elements (elements without the ability to support stresses) tend to become highly distorted, thus for presentation purposes, elements with accumulated plastic strains greater than 2.0 have not been drawn in the figure. From Fig. 8, we see that the model based on scaling laws offers less resistance to the plugging process (i.e., the fragment is penetrating faster). We also see that damage patterns between the two models differ. This is to be expected because the Johnson–Cook model is to some degree sensitive to hydrostatic conditions during the process of damage accumulation. Further, the Johnson–Cook model has been calibrated to a certain set of data while the scaling laws depend only on the homogeneous response of the material.

5. Discussion and conclusions

The current work is concerned with the description of a model for failure that is based on damage due to the process of adiabatic shear localization. We attempt to generalize scaling laws that are based on solutions to the problem of stress collapse during simple one-dimensional shear. By framing our model within the context of effective measures for stress and strain, damage due to shear becomes isotropic. We understand that this is not realistic but maintain that such methodology may prove quite effective. We note that for a broad class of problems that involve strong discontinuities and strongly driven boundary conditions (e.g., metal forming, metal cutting, impact, and penetration), loading in and around the failure region will not be significantly affected by such anisotropy. Because this generalization is perhaps the most significant assumption contained in the current framework, future work will most certainly focus on at least the simple incorporation of anisotropic damage due to the propagation of shear localization.

In order to develop a coherent numerical method, the model is parameterized only within the context of a single history variable, the local effective plastic strain. In this context the model assumes monotonic straining both approaching and beyond the peak stress. This simply is not the case for complex loading conditions. In other words, our model is independent of strain path and strain history and neglects loading that may be otherwise arrested or accelerated during the deformation history. Again, this can be an area of future work.

In order to determine the timing for stress collapse, the current formulation chooses to emphasize variations in the macroscopic flow field rather than variations in the internal material structure. The scaling laws provide insight as to how such variations could be combined as enhancing mechanisms for shear damage but we have chosen to emphasize the former over the latter and find value in this choice for a broad class of problems that are strongly driven by applied boundary conditions.

In the first example, that of monotonic compression, we see that without frictional effects our model is hard-pressed to determine material failure. We also know that at some point, some material imperfection will grow and propagate, ultimately resulting in failure. Modern techniques can offer much by way of characterization of the initial defects, and it would be tempting to develop a microstatistical description of such defect structure into an initial perturbation for the scaling laws (Eq. (6)). Since material variations and defects often occur at length scales directly influenced by the diffusive effects of heat conduction, such a framework should be approached with great caution. The point of this work, however, is to show that much can be done without reference to such detailed statistical characterization of materials. Further, by appealing to the homogeneous behavior of the material, the current model admits a great sensitivity to

hardening and softening mechanisms active within the material. A great variety of such mechanisms could be reflected in the homogeneous behavior by application of a more mechanism-based plasticity law. In this case however, we have limited ourselves to a very basic description of material behavior.

These points have been emphasized through example problems specifically designed to emphasize the strengths and weaknesses of the current formulation. Analysis of a simple compression specimen under a variety of frictional conditions was used to emphasize that the model is entirely dependent on variations in the velocity field that are driven entirely by macroscopic boundary conditions. As variations in deformation become stronger, and gradients higher, the local strain to failure decreases, and this becomes evident as the macroscopic strain to failure also decreases.

We compared our model to results from a highly resolved, and thus more fully physical, depiction of stress wave propagation away from an edge impact. In this case, we see that gross details of shear failure are well captured by our model while the finer details of stress decay prior to failure could be improved upon. Recent work (Bonnet-Lebouvier et al., 2002; Wright, 2003) is beginning to add insight to the velocity of shear band propagation and at some future date promises to influence the current model in this area.

Finally, we contrast our model to a widely exercised failure criterion first proposed by Johnson and Cook (1985) for the problem of a steel fragment incident on a Ti–6Al–4V plate. In this context, we find that both models depict failure via plate ''plugging'' but note that the current model does so without the benefit of prior experimental data for material failure. While the Johnson and Cook model carries the phenomenology of a broad experimental database (and thus provides information for a broad range of failure modes) our model presents the possibility of predicting failure only as a function of the homogeneous material behavior and the driving boundary conditions.

Acknowledgement

The authors acknowledge support from the Weapons and Materials Research Directorate of the Army Research Laboratory.

References

Bai, Y.L., 1982. Thermo-plastic instability in simple shear. Journal of the Mechanics and Physics of Solids 30, 195–207.

Bai, Y.L., Dodd, B., 1992. Adiabatic Shear Localization. Pergamon Press, Oxford.

Becker, R., 2002. Ring fragmentation predictions using the Gurson model with material stability conditions as failure criteria. International Journal of Solids and Structures 39, 3555–3580.

Bonnet-Lebouvier, A.S., Molinari, A., Lipinski, P., 2002. Analysis of the dynamic propagation of adiabatic shear bands. International Journal of Solids and Structures 39, 4249–4269.

Børvik, T., Hopperstad, O.S., Berstad, T., Langseth, M., 2002. Perforation of 12 mm thick steel plates by 20 mm diameter projectiles with flat, hemispherical and conical noses. Part II: numerical simulations. International Journal of Impact Engineering 27, 37–64.

Burkins, M.S., Love, W.W., Wood, J.R., 1997. Effect of annealing temperature on the ballistic limit velocity of Ti–6Al–4V ELI. ARL-MR-359.

Burkins, M.S., Hansen, J.S., Paige, J.I., Turner, P.C., 2000. The effect of thermo-mechanical processing on limit velocity of extra low interstitial titanium alloys. ARL-MR-486.

Clifton, R.J., 1980. Adiabatic shear banding. In: Materials Response to Ultra-High Loading Rates. NMAB-356. National Academy of Sciences, Washington, DC, NMAB-356.

Curran, D.R., Seaman, L., 1986. Computational models for nucleation, growth, and coalescence of adiabatic shear bands. In: Gupta, Y.M. (Ed.), Shock Waves in Condensed Matter. Plenum, New York, pp. 315–320.

Curran, D.R., Seaman, L., Shockey, D.A., 1987. Dynamic failure of solids. Physics Reports 147, 253–388.

Drucker, D.C., 1959. A definition of stable inelastic material. Journal of Applied Mechanics, Transaction of the American Society of Mechanical Engineers 81, 101–106.

Duffy, J., Chi, Y.C., 1992. On the measurement of local strain and temperature during the formation of adiabatic shear bands. Materials Science and Engineering A 157, 195–210.

Erlich, D.C., Seaman, L., Shockey, D.A., Curran, D.R., 1980. Development and application of a computational shear band model. BRL-CR-00416.

Grady, D.E., Kipp, M.E., 1987. The growth of unstable thermoplastic shear with application to steady-wave shock compression in solids. Journal of the Mechanics and Physics of Solids 35, 95–120.

Guduru, P.R., Rosakis, A.J., Ravichandran, G., 2001. Dynamic shear bands: an investigation using high speed optical and infrared diagnostics. Mechanics of Materials 33, 371–402.

Johnson, G.R., Cook, W.H., 1983. A constitutive model and data for metals subjected to large strains, high strain rates, and high temperatures. In: Proceedings of Seventh International Symposium on Ballistics, The Hague, The Netherlands, pp. 541–547.

Johnson, G.R., Cook, W.H., 1985. Fracture characteristics of three metals subjected to various strains, strain rates, temperatures and pressures. Engineering Fracture Mechancis 21, 31–48.

Johnson, G.R., Stryk, R.A., Holmquist, T.J., Beissel, S.R., 1997. Numerical Algorithms in a Lagrangian Hydrocode. WL-TR-1997-7093.

Kad, B.K., Schoenfeld, S.E., Burkins, M.S., 2000. Computational modeling of through-thickness dynamic impact response in cross-rolled Ti–6Al–4V plates. Metallurgical and Materials Transactions A 33A, 937–947.

Kalthoff, J.F., 2000. Modes of dynamic shear failure in solids. International Journal of Fracture 101, 1–31.

Li, Q.M., Jones, N., 2002. Response and failure of double-shear beam subjected to mass impact. International Journal of Solids and Structures 39, 1919–1947.

Magness, L.S., 1994. High strain rate deformation behaviors of kinetic energy penetrator materials during ballistic impact. Mechanics of Materials 17, 147–154.

Marchand, A., Duffy, J., 1988. An experimental study of the formation process of adiabatic shear bands in a structural steel. Journal of the Mechanics and Physics of Solids 36, 251–283.

Merzer, A.M., 1982. Modeling of adiabatic shear band development from small imperfections. Journal of the Mechanics and Physics of Solids 30, 323–338.

Molinari, A., Clifton, R.J., 1987. Analytical characterization of shear localization in thermoviscoplastic materials. Journal of Applied Mechanics 54, 806–812.

Raftenberg, M.N., 2001. A shear banding model for penetration calculations. International Journal of Impact Engineering 25, 123–146.

Raftenberg, M.N., Krause, C.D., 1999. Metallographic observations of armor steel specimens from plates perforated by shaped charge jets. International Journal of Impact Engineering 23, 757–770.

Rice, J.R., 1976. The localization of plastic deformation. In: Koiter, W.T. (Ed.), Proceedings of the 14th International Congress on Theoretical and Applied Mechanics. Noth-Holland Publishing Co., Amsterdam, pp. 207–220.

Saje, M., Pan, J., Needleman, A., 1982. Void nucleation effects on shear localization in porous plastic solids. International Journal of Fracture 19, 163–182.

Weerasooriya, T., Magness, L., Burkins, M.S., 2001. High strain-rate behavior of two Ti–6Al–4V alloys with different microstructures. In: Staudhammer, K., Murr, L., Meyers, M.A. (Eds.), Fundamental Issues and Applications of Shock-Wave and High-Strain-Rate Phenomena. Elsevier, Albuquerque, pp. 33–36.

Wright, T.W., 1990. Approximate analysis for the formation of adiabatic shear bands. Journal of the Mechanics and Physics of Solids 38, 515–530.

Wright, T.W., 1992. Shear band susceptibility: work hardening materials. International Journal of Plasticity 8, 583–602.

Wright, T.W., 1994. Toward a defect invariant basis for susceptibility to adiabatic shear bands. Mechanics of Materials 17, 215–222.

Wright, T.W., 2002. The Physics and Mathematics of Adiabatic Shear Bands. Cambridge University Press, Cambridge.

Wright, T.W., 2003. On the speed of an unconstrained shear band in a perfectly plastic material. International Journal of Solids and Structures 40, 871–879.

Wright, T.W., Batra, R.C., 1985. The initiation and growth of adiabatic shear bands. International Journal of Plasticity 1, 202–212.

Wright, T.W., Ockendon, H., 1996. A scaling law for the effect of inertia on the formation of adiabatic shear bands. International Journal of Plasticity 12, 927–934.

Xue, Q., Nesterenko, V.F., Meyers, M.A., 2001. Self-organization of shear bands in stainless steels: grain size effects. In: Staudhammer, K.P., Murr, L.E., Meyers, M.A. (Eds.), Fundamental Issues and Applications of Shock-Wave and High-Strain-Rate Phenomena. Elsever, Amsterdam, pp. 549–559.

Zener, C., Hollomon, J.H., 1944. Effect of strain rate upon plastic flow of steel. Journal of Applied Physics 15, 22–32.